

FINE-SCALE MEASUREMENTS OF TURBULENCE IN THE LOWER TROPOSPHERE: AN INTERCOMPARISON BETWEEN A KITE- AND BALLOON-BORNE, AND A HELICOPTER-BORNE MEASUREMENT SYSTEM

ANDREAS MUSCHINSKI¹, ROD FREHLICH², MIKE JENSEN², RON HUGO³,
AXEL HOFF⁴, FRANK EATON³ and BEN BALSLEY²

¹Cooperative Institute for Research in Environmental Sciences (CIRES), University of Colorado, and NOAA Environmental Technology Laboratory, 325 Broadway, Boulder, Colorado 80305-3328, U.S.A.

²Cooperative Institute for Research in Environmental Sciences (CIRES), University of Colorado, Boulder, Colorado 80309, U.S.A.

³U. S. Air Force Research Laboratory/DEBA, 3550 Aberdeen St., Kirtland Air Force Base, New Mexico 87117-5776, U.S.A.

⁴Aerodata Flugmeßtechnik GmbH, Hermann-Blenk-Straße 36, D-38108 Braunschweig, Germany

(Received in final form 24 March 2000)

Abstract. Two state-of-the-art, high-resolution, *in situ* turbulence measurement systems, which can be deployed at altitudes well above the atmospheric surface layer, are compared: the Tethered Lifting System (TLS) of the Cooperative Institute for Research in Environmental Sciences (CIRES) at the University of Colorado, Boulder, Colorado, and the helicopter-borne turbulence measurement system HELIPOD of the Technical University Braunschweig, Germany, and the University of Hanover, Germany. While the CIRES TLS is a fixed-point platform, HELIPOD is a moving platform. On the basis of data taken with the two systems in separate field campaigns, the system capabilities are quantified and discussed. Criteria for instrumental requirements are presented. It is shown that both the CIRES TLS and HELIPOD are well suited for measuring fine-scale turbulence that is characterized by very small temperature structure parameters (10^{-6} K² m^{-2/3} and smaller) and very small energy dissipation rates (10^{-7} m² s⁻³ and smaller). The authors are not aware of any other turbulence measurement systems that have similar capabilities and can be deployed at altitudes of up to several kilometres. The HELIPOD is ideal for high-resolution horizontal measurements while the TLS is ideal for high-resolution vertical measurements using multiple sensors attached to a suspended line.

Keywords: Airborne turbulence measurements, Energy dissipation rate, Fine-wire anemometry, Fine-wire thermometry, HELIPOD, Structure parameters, Tethered Lifting System.

1. Introduction

Above the atmospheric surface layer (ASL), particularly in the nocturnal boundary layer (NBL), in the residual layer, and in the free atmosphere, turbulence is typically weak and intermittent. In the stably stratified atmosphere far from the surface, there is a complicated interplay between convective and dynamical instabilities and the generation and evolution of small-scale turbulence. This makes the validity of



traditional simple parameterization schemes such as flux-profile and flux-variance relationships questionable.

A major goal of present-day meteorology is to deepen the physical understanding of the interaction between low-level, mesoscale phenomena (gravity waves, mountain waves, density currents, low-level jets) and small-scale turbulence in the NBL. Two measurement systems that have the potential to provide unique *in situ* observations for such research are the Tethered Lifting System (TLS) of the Cooperative Institute for Research in Environmental Sciences (CIRES) at the University of Colorado, Boulder, and the helicopter-borne turbulence measurement system HELIPOD. The CIRES TLS has been jointly developed by scientists at the U.S. Air Force (USAF) and at CIRES, University of Colorado. HELIPOD was jointly developed by Aerodata Flugmeßtechnik GmbH, Braunschweig, Germany, the University of Hanover, Germany, and the Technical University of Braunschweig, Germany.

The purpose of this paper is twofold: (i) to provide quantitative evidence that both airborne instruments are capable of measuring characteristics of very weak turbulence with high spatial resolution; and (ii) to present a set of instrumental requirements that need to be fulfilled when airborne sensors are deployed for measuring small-scale turbulence.

The paper is organized as follows. In Section 2, we describe the CIRES kite and blimp system and HELIPOD in some detail. Section 3 provides the theoretical basis for retrieving turbulence structure parameters from measured time series of turbulent quantities. In Section 4, sample data are presented that demonstrate the capability of both systems to measure weak turbulence. A discussion is given in Section 5, and Section 6 contains a summary and conclusions.

2. Instrumentation

In this section, we first give a general overview of the advantages and disadvantages of fixed-point turbulence measurements over aircraft-borne* turbulence measurements and vice versa. In the second and third parts, we describe the CIRES kite and blimp systems and the helicopter-borne turbulence instrument HELIPOD, respectively.

* Here we use the term 'aircraft-borne' instead of 'airborne', in order to clearly distinguish between measurements onboard aircraft (fixed-wing aircraft and helicopters) and measurements collected with balloons, blimps, and kites. That is, we use the more general term 'airborne' for measurements onboard aircraft as well as for measurements using tethered balloons, blimps, and kites.

2.1. FIXED-POINT VERSUS AIRCRAFT-BORNE TURBULENCE MEASUREMENTS – A BRIEF OVERVIEW

Fixed-point turbulence measurement systems such as those mounted on the ground, on towers, blimps, and kites allow one to measure turbulence quantities only along the mean wind direction, thereby making use of Taylor's frozen turbulence hypothesis (Taylor, 1938), which forms the basis for converting a time series of a fluctuating quantity into a spatial series of fluctuations along the direction of the mean wind. Taylor's hypothesis, however, is not applicable if the turbulent fluctuations of the wind velocity are comparable to or even exceed the mean wind velocity. Within limitations, there are correction schemes for Taylor's hypothesis (e.g., Wyngaard, 1986).

There is a long tradition of fixed-point measurements in the atmospheric surface layer, which typically comprises the lowest 50 m of the Earth's atmosphere (e.g., Friehe, 1986; Kaimal, 1986). The well-known Kansas experiment (Kaimal et al., 1972) relied on fixed-point measurements and is generally considered the *experimentum crucis* that proved the validity of Monin–Obukhov scaling in the surface layer under a wide range of meteorological conditions.

In addition, fixed-point measurements on tall towers have provided significant insight into the turbulence characteristics well above the surface layer (Kaimal and Gaynor, 1983; Angevine et al., 1998) but towers are limited to heights of about 500 m. Towers with heights exceeding 100 m are practically non-portable, which makes them inappropriate for deployment on a campaign basis, in particular at remote locations. The logistical limitations of towers can partly be overcome by using tethered balloons (e.g., Kaimal et al., 1976; Ogawa and Ohara, 1982) and blimps and kites (e.g., Balsley et al., 1992). With modern kite and blimp technology, the altitude range from the top of the surface layer up to several kilometres can be covered. A disadvantage of these systems, however, is their relatively small payload and small power capabilities.

Parallel with the development of aircraft, there has been a continuous development of meteorological measurement systems onboard aircraft (e.g., Lenschow, 1972; Vörsmann, 1984; Hauf, 1984; Lenschow, 1986; Crawford and Dobosy, 1992). Meteorological measurements onboard aircraft are in many respects complementary to fixed-point measurements. Aircraft have the following advantages: they can fly in directions transverse to the mean wind; compared to kites and balloons, they can carry heavy payloads; they can easily change altitude*; they can be operated between tens of metres and many kilometers above the ground; they can fly in patterns that cover an area, thereby being more appropriate than fixed-point platforms for measurements of areal averages of turbulent quantities. But there are also disadvantages: compared to fixed-point instrumentation, the

* It has to be pointed out, however, that sensor altitudes can be quickly changed also by means of a carriage mounted at a tower, or by the WindTRAM, which is part of the CIRES TLS described later in this paper.

operation of an aircraft is relatively expensive and limited in time; true vertical profiling is not possible, except by using dropsondes that can be released from aircraft; measurements at different altitudes at the same time are not possible; the relatively high true air speed requires a higher sampling frequency; secondary effects like vibration, adiabatic heating at the sensor, and flow distortion close to the aircraft's body become important; sophisticated navigation systems for orientation and position measurements are required in order to reliably transform the velocity vector measurements from an aircraft-fixed coordinate system into an earth-fixed coordinate system.

Most aircraft-borne meteorological instrumentation is operated onboard fixed-wing aircraft. As an alternative, one can also equip a suitably small pod that hangs at a sufficient distance below the aircraft. This solution reduces the contaminating effects of engine vibration and flow distortion but, on the other hand, sets additional requirements regarding sensor miniaturization, maneuverability, and the measurement of orientation and position that needs to be done inside the pod. HELIPOD (Muschinski and Wode, 1998) is a turbulence measurement system that is operated below a helicopter. To the authors' knowledge, HELIPOD is the only existing state-of-the-art helicopter-borne turbulence instrument, and it will be described in Section 2.3.

2.2. THE CIRES KITE AND BLIMP SYSTEMS

2.2.1. *Platform Concept*

Over the last decade, researchers at the Cooperative Institute for Research in Environmental Sciences (CIRES) at the University of Colorado in the USA have developed complementary tethered kite and blimp systems for atmospheric research. A brief description of these systems is given here, but we refer the reader to Balsley et al. (1998) and Knapp et al. (1998) for more detailed descriptions. These systems are designed to lift modest (5–10 kg) payloads through the boundary layer and lower free troposphere under a wide range of wind conditions, while remaining portable and cost-effective. The kite and blimp systems share many common components including winches, tethers, and payloads.

For the field campaign described in this paper (during spring 1998 at the White Sands Missile Range, New Mexico), we used the rear drive wheel of a vehicle raised off the ground as the motive power for raising and lowering both the kites and the blimp. An automated take-up reel that used 12-volt battery power was supplied by the vehicle to spool the Kevlar tether. During the first day of the experiment under moderate wind conditions, we used a 7.4 m² parafoil kite for our observations. The remainder of the week-long campaign, however, saw much lower winds and therefore a 21 m³ polyurethane blimp was used (see Figure 1). In general, blimps are employed when the winds are less than about 7–8 m s⁻¹, while kites (Figure 2) are used for winds above that value.



Figure 1. The CIRES blimp.

Payloads were suspended from a long line suspended from the tether when the kite platform was used. During the blimp-borne measurements the payload was attached in series with the tether and well below the blimp (Figure 3). A special line attachment was designed for use with the blimp to allow the payload turbulence probes to orient themselves into the wind, independent of the angle of the tether line. Figure 4 shows the payload that carries the CIRES sensors (a thermocouple temperature sensor and a Pitot tube).

In addition to the turbulence sensors described below, a basic meteorological payload consisting of a Vaisala RS-80 radiosonde and Tmax-board interface was flown. This system allowed us to transmit real-time measurements of pressure, temperature, and humidity (and potentially five additional sensor channels) down from the payload package roughly once every seven seconds. For this experiment, additional sensors included wind speed and direction, solar radiation, and payload pitch and roll angles.



Figure 2. One of the kites that has been used as part of the CIRES kite and blimp system.

2.2.2. Sensors

Two different sets of temperature and velocity sensors have been deployed with the kite/blimp systems: thin-wire probes provided by the U.S. Air Force (USAF), and more conventional sensors (thermocouple and Pitot tube) developed and calibrated at CIRES. In the following, we first describe the USAF sensors as used and calib-



Figure 3. The CIRES/USAF sensor array, suspended below the CIRES blimp. The uppermost package is the basic meteorology payload, in the middle is the USAF sensor package (hot-wire and cold-wire sensors), and at the bottom there is the CIRES sensor package (thermocouple sensor and Pitot tube). The CIRES package hangs 2.95 m below the basic meteorology payload.

rated for the April 1998 field experiment; second, we give a brief presentation of the CIRES sensors.

The Air Force sensor package consisted of a constant-temperature anemometer (CTA) operated at a high overheat ratio and a constant-current anemometer (CCA) operated as a resistance thermometer at a low overheat ratio. The anemometer sensor consisted of two 5- μm platinum-plated tungsten wires (DISA 55P52 probe),



Figure 4. The CIRES sensor payload, which includes a Pitot tube and a thermocouple sensor.

each 3 mm in length with the middle 1.25 mm exposed to the flow and the remaining length coated with a 0.5- μm thick fused silica coating. The wires were mounted at 90 degrees to the flow and at right angles to each other and separated in the streamwise direction by approximately 5 mm. The upstream wire was operated in constant-current mode and the downstream wire in constant-temperature mode. This arrangement kept the thermal wake of the CTA from interfering with the temperature measurements of the CCA. The CCA was operated in what is often referred to as the low-overheat mode with a fixed current of 2 mA.

The anemometer circuits were designed in-house for low-current battery operation. The AC channel of the CTA was conditioned with a second-order high-pass filter at 0.01 Hz and a fourth-order low-pass filter at 50 Hz, amplified by 34.8. The AC channel of the CCA was conditioned with a first-order high-pass filter at

0.01 Hz and a fourth-order low-pass filter at 50 Hz, and then amplified by 51,128. The two AC channels were sampled at 50 s^{-1} and the two DC channels at 0.5 s^{-1} .

The coefficients of thermal resistivity (α_{20}) of the wires were determined by placing the wires in an environmental chamber along with a reference thermocouple, reducing the temperature to -60°C and then allowing the chamber to return to room temperature over a period of approximately four hours. The coefficient of thermal resistivity was used with Equation (1) and the measured resistance R_T to determine T , the temperature fluctuation time history. The mean DC temperature was obtained using the sensor in the radiosonde package,

$$R_T = R_{20} [1 + \alpha_{20} (T - T_{20})]. \quad (1)$$

The calibration (Hugo et al., 1999) of the CTA for velocity was performed *in situ* by referencing the CTA mean voltages to the mean velocity from the CIRES Pitot-static tube and the mean pressure from the radiosonde. A form of King's law (King, 1914) was used to relate the convective heat transfer coefficient to the flow Reynolds number,

$$\text{Nu} = a + b (\text{Re})^n, \quad (2)$$

where $\text{Nu} = \frac{hd_w}{k_f}$ is the Nusselt number with h the convective heat transfer coefficient, d_w the wire diameter, k_f the thermal conductivity of air, $\text{Re} = \frac{\rho_f V d_w}{\mu_f}$ the Reynolds number, ρ_f the density of air, V the speed of the flow over the wire, and μ_f the dynamic viscosity of air. The subscript f refers to properties being evaluated at the film temperature of the wire, which is the average of the ambient temperature and the wire temperature ($T_f = \frac{T_\infty + T_w}{2}$). Cimbala and Park (1990) with modification by Cardell (1993) describe procedures for determining the values of coefficients a , b , n , and T_w in Equation (2).

Upon determining the values of a , b , n , and T_w , the time history of velocity fluctuations can be computed using Equation (3) with R the ideal gas constant, P_{atm} the local atmospheric pressure, E_{hw} the voltage across the hot wire, R_w the resistance of the hot-wire at its operating temperature T_w , and l_w the length of the wire,

$$V = \frac{RT_f \mu_f}{P_{atm} d_w} \left[\left(\frac{E_{hw}^2}{\pi R_w l_w k_f (T_w - T_{atm})} - a \right) \frac{1}{b} \right]^{\frac{1}{n}}. \quad (3)$$

Use of Equation (3) requires the fluctuating temperature time series and hot-wire voltage time series as inputs. As described in Paranthoen et al. (1982) and Bruun (1995), the temperature time series need not be compensated for probe-prong conduction effects prior to use in Equation (3) provided that similarly constructed wires are used for both the hot-wire and the cold-wire, which is the case for the Dantec 55P52 sensor used in this study. In addition, it was not necessary to compensate for the thermal inertia of the wire as the 3 dB point for the lowest velocities

was around 108 Hz, which is well above the low-pass filters used to condition the CCA signal.

When using the temperature time series for the evaluation of temperature fluctuations alone, it is necessary to compensate for the effects of probe-prong conduction. This was not done with the data in the present investigation because two existing models (Paranthoen et al., 1982, 1983; Tsuji et al., 1992; Nagano and Tsuji, 1994) used to predict the amount of attenuation did not agree. One model (Paranthoen et al., 1982, 1983) predicted attenuations on the order of 90% and the other model (Tsuji et al., 1992; Nagano and Tsuji, 1994), which accounts for the 0.5- μm thick fused silica coating on the wire, predicted no attenuation at all.

High-resolution temperature for deriving the turbulence structure parameters of temperature and refractive index has been measured by the USAF to assess the optical turbulence properties of the atmosphere for several years, with particular attention paid to the turbulence found in the upper troposphere and the stratosphere (Masson et al., 1996). Measurements have been taken with a sampling rate of 12 kHz using a C-135E or Gulfstream II aircraft flying at about 220 m s⁻¹. These measurements were compared to VHF radar observations (Eaton et al., 1998) and ground-based scintillometer measurements (Hahn et al., 1999). The same temperature sensors used on the aircraft were mounted on the CIRES kite and blimp system described in this paper.

The thin-wire technique has been widely used for high-resolution measurements in the atmospheric surface layer. On tethered balloons, blimps, kites, and in particular onboard aircraft, however, it is typical to use more robust and slower responding sensors. In the remainder of this subsection, we describe the CIRES sensors.

The thermocouple probe is an inexpensive type E bead thermocouple with 25- μm diameter wire. At room temperature, the type E thermocouple has the highest Seebeck coefficient ($\alpha \approx 60 \mu\text{V K}^{-1}$) of all common thermocouples and is therefore relatively sensitive. A calibration curve for the thermocouple probe was provided by the manufacturer. The resistance of the probe was reduced to approximately 10 Ω by mounting a 1-cm section of the fine-wire thermocouple onto a heavy gauge E thermocouple wire. The spectral level of the thermally induced voltage noise from the probe is then $S_U^{(n)} = 1.6 \times 10^{-7} \mu\text{V}^2 \text{ Hz}^{-1}$. The noise floor in the measured temperature spectrum is $S_{T,m}^{(n)} = 4.44 \times 10^{-11} \text{ K}^2 \text{ Hz}^{-1}$ at a bandwidth of 25 Hz. This performance could be achieved with very low-noise amplifiers. The current design is limited by the additive noise of the first amplifier and produces a noise floor in the measured temperature spectrum of $S_{T,m}^{(n)} = 2.8 \times 10^{-10} \text{ K}^2 \text{ Hz}^{-1}$. The frequency response of the probe is

$$\frac{S_{T,m}(f)}{S_T(f)} = q(f) = \left(1 + \frac{f^2}{f_0^2}\right)^{-1} \left(1 + \frac{f^2}{f_1^2}\right)^{-1} \left[\frac{f^2}{f_2^2} \left(1 + \frac{f^2}{f_2^2}\right)^{-1}\right], \quad (4)$$

where $f_0 \approx 10 \text{ Hz}$ is the 3-dB bandwidth of the bead thermocouple, $f_1 = 25 \text{ Hz}$ is the 3-dB bandwidth of the anti-alias filter, which was chosen to match the sampling

frequency of 50 Hz, and $f_2 = 0.0159$ Hz is the 3-dB bandwidth of the high-pass filter. That is, at a Nyquist frequency of $f_{Ny} = 25$ Hz, we have $q(25 \text{ Hz}) = 0.069$, which leads to a true temperature noise floor of $S_T^{(n)} = 4.1 \times 10^{-9} \text{ K}^2 \text{ Hz}^{-1}$, corresponding to an uncorrelated noise temperature standard deviation of 0.32 mK.

A 12-bit digitizer sampled the temperature sensor signal with a resolution of $\Delta T = 0.4882$ mK. The contribution to a measured temperature variance from the digitizer resolution is $\Delta T^2/12$ (Oppenheim and Schaffer, 1975), which is equivalent to a constant spectral noise floor in the measured spectrum $S_{T,m}(f)$ of $S_{T,m}^{(n)} = \Delta T^2/(12f_{Ny}) = 0.794 \times 10^{-9} \text{ K}^2 \text{ Hz}^{-1}$, which, at $f_{Ny} = 25$ Hz, corresponds to a true spectral noise density of $S_T^{(n)} = 1.15 \times 10^{-8} \text{ K}^2 \text{ Hz}^{-1}$. That is, close to f_{Ny} the quantization noise exceeds the amplifier noise in the reconstructed, true temperature spectrum $S_T(f)$.

A robust Pitot-tube velocity sensor was developed to measure small-scale velocity turbulence. A 15-cm-long tube was oriented into the mean wind with a long vane. The dynamic pressure was measured with a Data Instruments Model XPC pressure sensor. A low-noise preamp with a gain of 2000 converted the pressure signal into a detectable voltage signal with a sensitivity of $0.02196 \text{ V Pa}^{-1}$. The dynamic pressure P is related to the velocity by $P = \rho V^2/2$, where ρ is the density of air. The main engineering challenges are the removal of sensor drift from temperature and mean pressure measurements, and reducing the level of the spectral noise floor.

2.3. THE HELICOPTER-BORNE TURBULENCE MEASUREMENT SYSTEM HELIPOD

2.3.1. Platform Concept

HELIPOD (Figure 5) is a helicopter-borne system for *in situ* high-resolution measurements of atmospheric turbulence. It operates as a tethered external load under its carrier system. Its basic principle of instrumentation is similar to that on fixed-wing aircraft with *in situ* turbulence equipment. HELIPOD was developed during the early 1990s jointly by scientists and engineers at the University of Hannover, Germany, the Technical University Braunschweig, Germany, and at Aerodata Flugmeßtechnik GmbH, Braunschweig, Germany.

The main motivation for the development of HELIPOD came from the scientific and logistical requirements for micrometeorological measurements in the polar and tropical regions. In contrast to typical fixed-wing aircraft, helicopters can be operated from a ship. This can be a major advantage of a helicopter-borne system if the measurement site is hundreds or even thousands of kilometres away from the nearest airport. Although long-range aircraft can also operate in remote areas, operating from a ship can offer more flexibility. Additionally, HELIPOD can be operated at lower altitudes (down to less than 10 m) and at lower forward velocities (typically 40 m s^{-1}) than all fixed-wing aircraft that are used for meteorological measurements. This relaxes the situation for sampling small-scale turbulence close



Figure 5. The helicopter-borne turbulence measurement system HELIPOD. The photograph was taken during a field experiment in the Arctic.

to the ground, which is necessary especially in very stably stratified regions such as the polar regions where the boundary layer is often very shallow.

HELIPOD has a mass of about 250 kg and is operated on a tether 15 m below a helicopter. The length of the tether has been chosen to be long enough such that at a forward velocity of 40 m s^{-1} , which must be maintained in order to keep the pod aerodynamically stable, the downwash from the rotor has negligible effect on the measurements.

In addition to meteorological sensors for pressure, temperature, three-dimensional velocity vector, and humidity, HELIPOD is equipped with two Global Positioning System (GPS) receivers (both NovAtel GPSCardTM as a 10-channel C/A code unit with carrier phase output), a Litton LCR 88 AHRU inertial navigation system (INS), and a radio altimeter. The GPS and INS data are jointly processed in a navigation data-processing routine that provides a position and attitude history combining the high absolute accuracy of GPS with the fast response of the INS data. The processed GPS/INS data are sampled at 50 Hz.

On a higher level, the navigational and meteorological data are jointly processed in real time, such that the instantaneous wind vectors are immediately available in an earth-fixed coordinate system. Off-line processing using data from additional GPS receivers on the ground provides HELIPOD positions with an absolute accuracy of better than 5 m.

2.3.2. *Sensors and Real-Time Processing*

HELIPOD contains a number of meteorological sensors and a computing system (VME bus board computer system, Aerodata AD-VC 6) for acquisition, temporal coordination, and storage of the raw data and for the real-time processing and real-time visualization of the final meteorological data. Data for static pressure, three-dimensional wind vector, temperature, and humidity are obtained at a sampling rate of 100 Hz, so that at a true air speed of 40 m s^{-1} the horizontal spacing is 40 cm.

A five-hole probe (Rosemount 858 AJ) is used for measuring static, dynamic, and differential pressures in the vertical and transverse directions, respectively. The transducers for total (Setra 270) and differential pressures (Setra 239) have been chosen for their short response time (less than 10 ms) and high accuracy.

Two different temperature sensors are used: a system for measuring high-frequency fluctuations (Aerodata AD-STs) and a conventional sensor for measuring the absolute temperature at lower frequencies (Rosemount 102 BW).

Aerodata AD-STs (Figure 6), developed especially for HELIPOD, was designed to minimize errors due to self-heating, infrared radiation, local recovery effects (e.g., Lenschow, 1986, p. 42), and the boundary layer within the housing, such that the combined uncertainty would not exceed 5 mK. The system consists of a tube with an internal diameter of 55 mm completely open in the air-flow direction. The rear outlet can be changed to reduce the air speed inside the tube to a value in a range between 2 m s^{-1} and 5 m s^{-1} . This gives a recovery factor of nearly unity, which is closely equivalent to adiabatic warming. At higher speeds, the temperature distribution around the sensor element increases to an amount that would be difficult to calculate. An additional internal tube is employed for two purposes. First, there is an additional reduction of possibly varying infrared heating by radiation fluctuations on the housing. Second, and more important, there is an additional flow alignment for a local pressure measurement very close to the temperature probe. This allows measurement of the instantaneous recovery effect of the complete housing instead of assuming it to be constant (Lenschow, 1986, p. 42).

The fast-response temperature sensor element (Figure 7) consists of a $5\text{-}\mu\text{m}$ tungsten wire with a length of 20 mm. It is carried on a quickly interchangeable small support on top of a manually moveable insert. The zigzag wire, which has a resistance close to 50Ω at 0°C , is suspended by six prongs perpendicular to the air flow and connected in a four-wire bridge configuration to a high-performance signal-conditioning unit. The time constant of the sensor element itself is on the order of a few milliseconds.

The humidity is measured with three different hygrometers, which cover three different but overlapping frequency ranges: a dew point, a capacitive, and a Lyman- α hygrometer. The capacitive and the Lyman- α hygrometers are integrated in a chamber having a short inlet pipe through HELIPOD's nose cone (Buck Research/Aerodata HMS-1). The chamber's outlet has a hot-wire flow probe for

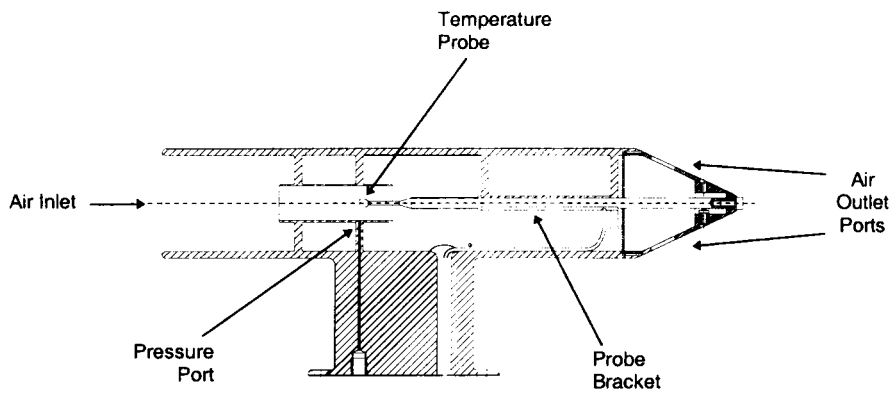


Figure 6. HELIPOD's fast-response temperature sensor system AD-STs.

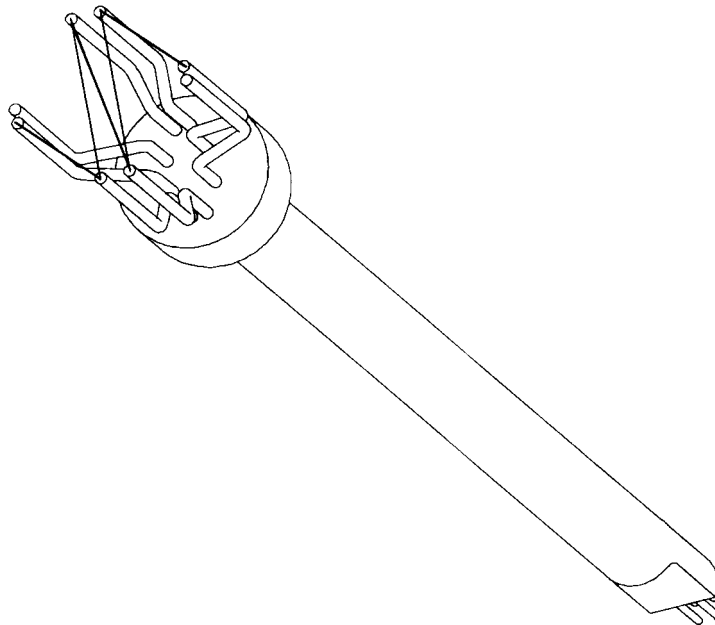


Figure 7. Detailed view of HELIPOD's 5- μm fine-wire temperature sensor element, labeled as 'temperature probe' in Figure 6.

adjusting the internal flow to about 10 m s^{-1} . Pressure and temperature inside the chamber are measured. The humidity sensor system is shown in Figure 8.

The high-frequency humidity signal is measured with the Lyman- α -hygrometer (Buck, 1976). The lower-frequency fluctuations are measured with an appropriately adapted capacitive humidity sensor (Vaisala Humicap), which is combined with a thermometer. The dew point hygrometer (General Eastern 1011 B) is used for off-line check and calibration. It is located in a bypass close behind the main chamber containing the capacitive and the Lyman- α hygrometers. The pressures in the main

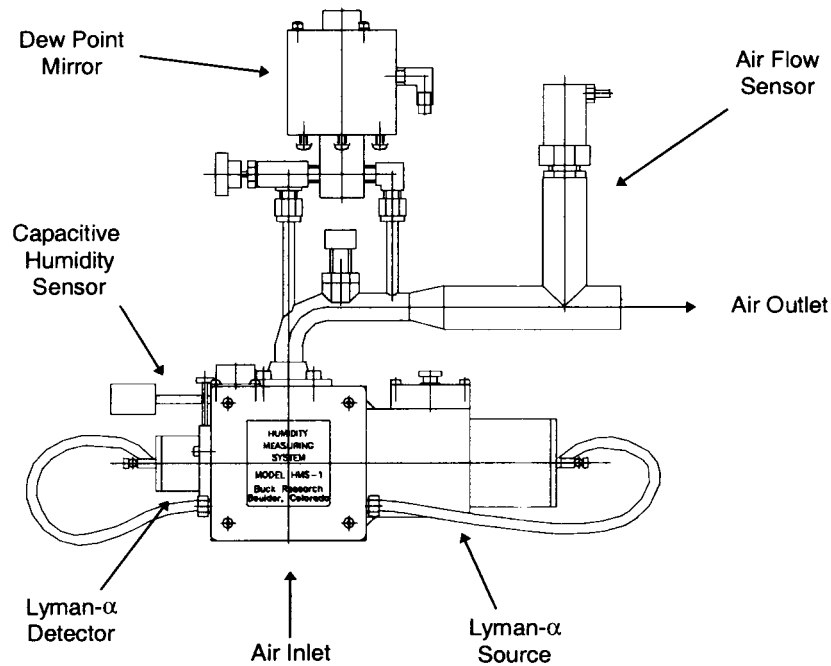


Figure 8. HELIPOD's humidity sensor system, consisting of a dew point mirror, a capacitive sensor (Humicap), and a Lyman- α hygrometer.

chamber and at the dewpoint hygrometer can differ from each other. Thus, two pressure sensors are used.

A downward looking radiation thermometer (Heimann KT 19) measures the surface radiation temperature. A radio altimeter provides the distance to the ground with an accuracy as small as 1 m, depending on the terrain and HELIPOD's attitude.

On the basis of the differential pressure sounding in the AD-STs and the correct dynamic pressure value, the fluctuating component of the total temperature can be calculated exactly. The low-frequency component of the total temperature is measured with a standard Rosemount sealed-element aviation thermometer. A numerical complementary filter algorithm is applied for properly merging the low-frequency with the high-frequency component. This is done in order to minimize the influence of a long-term drift of the open $5\text{-}\mu\text{m}$ tungsten wire, which can be caused by dust and salt contamination. The static temperature is then calculated from the total temperature, and the dynamic and static pressures.

In the real-time data-processing system, the Lyman- α and humicap data are used in a similar way for the calculation of drift-free and fast-response humidity data. The barometric altitude is updated in real time on the basis of the instantaneous values of static temperature, static pressure, and humidity.

The wind vector (Lenschow, 1972, 1986, pp. 39ff.; Vörsmann, 1984) is calculated in several steps. First, the static and dynamic pressures, total temperature, and humidity provide the true airspeed. Based on the angles of attack and sideslip, the air velocity vector in the local coordinate system is determined. Using the attitude angles of the navigation system, this vector is transformed into the earth-fixed coordinate system.

HELIPOD's vertical velocity in an earth-fixed coordinate system (the 'vertical inertial velocity') is calculated from both barometric altitude increments and data from the INS/GPS system (Redeker and Vörsmann, 1985), thereby making optimum use of the two data streams. The INS/GPS also provides the horizontal components of the inertial velocity, such that the wind vector in an earth-fixed coordinate system can be calculated as the vector difference between the wind vector in the HELIPOD-fixed system and HELIPOD's inertial velocity vector.

3. Instrument Requirements for Inertial-Range Turbulence Measurements from Moving Platforms

Consider a time series of a fluctuating, real quantity, $q(t)$, whose mean value is zero. Let V be the mean relative speed between the sensor and the air, which is also called the 'true air speed'. Then a time lag τ corresponds to the spatial lag

$$\lambda = V\tau, \quad (5)$$

and the frequency $f = 1/\tau$ corresponds to the wavenumber

$$k = \frac{2\pi}{\lambda} = \frac{2\pi}{V\tau} = \frac{2\pi}{V}f. \quad (6)$$

The relationship between the one-sided frequency spectrum $S_q(f)$ and the one-sided, one-dimensional wavenumber spectrum $F_q(k)$ is given by

$$F_q(k) dk = S_q(f) df, \quad (7)$$

that is,

$$F_q(k) = S_q(f) \frac{df}{dk} = S_q(f) \frac{V}{2\pi}. \quad (8)$$

On the basis of classical inertial-range turbulence theory (see Appendix A), we know

$$F_q(k) = 0.249C_q^2 k^{-\frac{5}{3}}. \quad (9)$$

It follows that the structure parameter can be expressed as function of frequency spectral density, frequency, and true air speed as follows,

$$C_q^2 = 4.016 S_q(f) f^{\frac{5}{3}} \left(\frac{2\pi}{V} \right)^{\frac{2}{3}} = 13.67 S_q(f) f^{\frac{5}{3}} V^{-\frac{2}{3}}. \quad (10)$$

For many turbulence problems, the small-scale spatial statistics are well described by an inertial-range spatial spectrum, and the level of the spectrum is given by important turbulence parameters such as the energy-dissipation rate ε for velocity spectra or the temperature structure parameter C_T^2 for the temperature spectrum. Measurement of a one-dimensional, spatial spectrum requires sampling the spatial spectrum over a wavenumber interval (k_1, k_2) , where

$$k_1 = \frac{2\pi}{L} \quad (11)$$

is the smallest wavenumber of interest and

$$k_2 = \frac{2\pi}{l} \quad (12)$$

is the highest wavenumber that must be observed. The instrumental requirements for three different given true air speeds V are shown in Figure 9. The spatial wavenumber region $k_1 = \frac{2\pi}{L}$, $k_2 = \frac{2\pi}{l}$ maps into the temporal frequency region $(f_1, f_2) = (k_1 \frac{V}{2\pi}, k_2 \frac{V}{2\pi})$. The most critical instrument requirements are the highest frequency that can be measured (frequency bandwidth) and sampled, and the spectral level of the instrument noise, which is typically a constant, i.e., uncorrelated white noise.

Figure 9 illustrates that the required bandwidth increases and the required noise floor decreases with increasing true air speed. That is, the same sensor generally provides higher-resolution turbulence spectra when carried on a slowly moving platform.

Let us now require that for a given structure parameter C_q^2 , a given true air speed V , a given length l (which defines the upper boundary of the wavenumber interval that is to be measured), the Nyquist frequency and the sensor's bandwidth be sufficiently high and the sensor's noise floor be sufficiently low that the inertial-range spectrum can be observed up to the wavenumber k_2 and the spectral density at k_2 is not smaller than the sensor's noise floor, $S_q^{(n)}$.

The criterion for the minimum Nyquist frequency and the minimum bandwidth is

$$f_{Ny} \geq \frac{V}{2\pi} k_2 = \frac{V}{l}. \quad (13)$$

The criterion for the maximum allowable noise floor in the frequency spectrum is

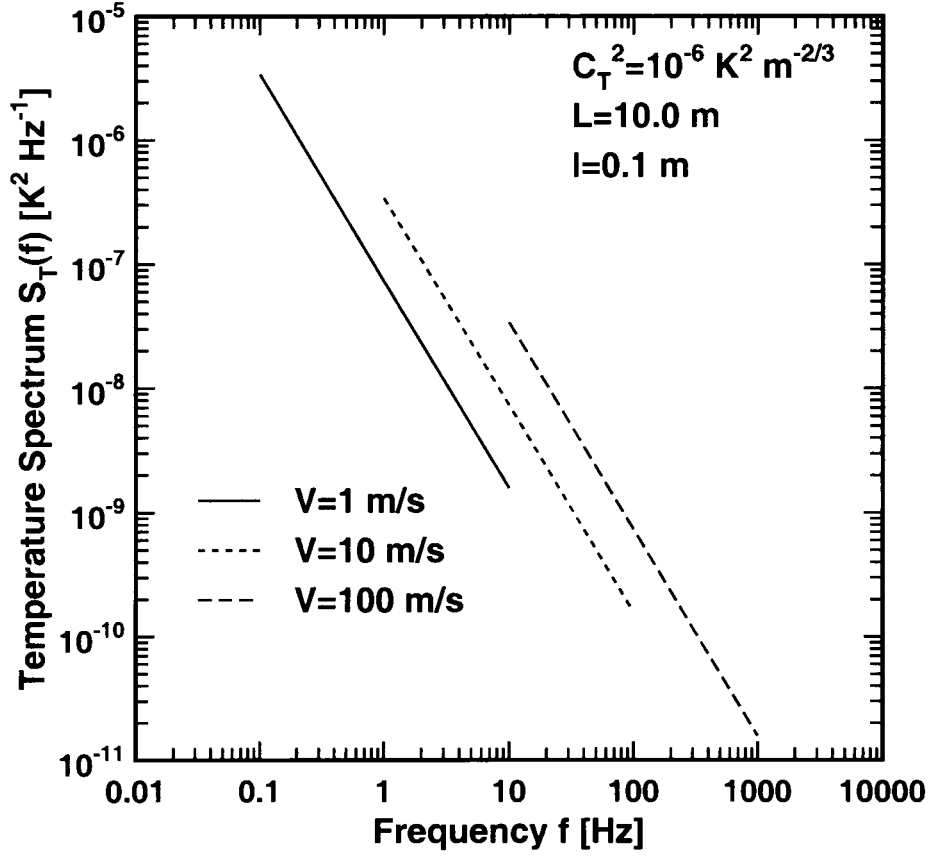


Figure 9. The purpose of the figure is to illustrate the mapping from a wavenumber interval $k_1 = 2\pi/L$, $k_2 = 2\pi/l$ into a frequency interval $f_1 = k_1(V/2\pi)$, $f_2 = k_2(V/2\pi)$ as described in Equations (11) and (12) and in the text thereafter. Model frequency spectra of turbulent temperature fluctuations for a given structure parameter ($C_T^2 = 10^{-6} \text{ K}^2 \text{ m}^{-2/3}$) are shown but for three different given true air speeds V (1 m s^{-1} , 10 m s^{-1} , and 100 m s^{-1}). The spectra are shown such that the wavelength interval between $l = 0.1 \text{ m}$ and $L = 10 \text{ m}$ is sampled. Here, we have chosen l and L such that the wavelength interval is of practical relevance for measurements of inertial-subrange turbulence in the stably stratified atmosphere.

$$S_q^{(n)} \leq \frac{2\pi}{V} F_q(k_2) = 0.249 \frac{2\pi}{V} C_q^2 \left(\frac{2\pi}{l} \right)^{-\frac{5}{3}} = 0.0731 C_q^2 l^{\frac{2}{3}} \tau, \quad (14)$$

where

$$\tau = \frac{l}{V} \quad (15)$$

is the time needed to sample the length l at the true air speed V . That is, resolving the temperature inertial-range spectrum down to $l = 1$ m in the case of a structure parameter $C_T^2 = 10^{-6} \text{ K}^2 \text{ Hz}^{-2/3}$ requires a noise floor that does not exceed $7.31 \times 10^{-8} \text{ K}^2 \text{ Hz}^{-1}$ if $V = 1 \text{ m s}^{-1}$ and a noise floor that does not exceed $7.31 \times 10^{-10} \text{ K}^2 \text{ Hz}^{-1}$ if $V = 100 \text{ m s}^{-1}$; see Figure 9.

Inserting the relationships between the structure parameters of the longitudinal velocity, C_u^2 , and the vertical velocity, C_w^2 , and the energy dissipation rate ε , i.e., Equations (31) and (32), leads to noise floor criteria for the longitudinal velocity measurements,

$$S_u^{(n)} \leq 0.15(\varepsilon l)^{\frac{2}{3}} \tau \quad (16)$$

and for the vertical velocity measurements,

$$S_w^{(n)} \leq 0.20(\varepsilon l)^{\frac{2}{3}} \tau, \quad (17)$$

respectively. That is, for $l = 1$ m, $V = 1 \text{ m s}^{-1}$ (100 m s^{-1}), and $\varepsilon = 10^{-6} \text{ m}^2 \text{ s}^{-3}$, the longitudinal and vertical velocity noise floors must not exceed $1.5 \times 10^{-7} \text{ m}^2 \text{ s}^{-2} \text{ Hz}^{-1}$ ($1.5 \times 10^{-9} \text{ m}^2 \text{ s}^{-2} \text{ Hz}^{-1}$) and $2.0 \times 10^{-7} \text{ m}^2 \text{ s}^{-2} \text{ Hz}^{-1}$ ($2.0 \times 10^{-9} \text{ m}^2 \text{ s}^{-2} \text{ Hz}^{-1}$), respectively.

In the next two sections, we will discuss to what extent the CIRES TLS and HELIPOD fulfill these criteria.

4. Two Case Studies

In this section, we present results from high-resolution turbulence measurements above the ASL obtained in two different field experiments. First, we present measurements taken with the CIRES kite and blimp system during the April 1998 field experiment at White Sands Missile Range (WSMR), New Mexico. Second, we show data obtained with HELIPOD during the Profiler-HELIPOD Intercomparison Experiment (PHELIX) conducted in November 1997 at Vandenberg Air Force Base in the California Central Coast.

4.1. MEASUREMENTS IN THE RESIDUAL LAYER USING THE CIRES KITE AND BLIMP SYSTEM

A blimp flight was conducted on 29 April 1998 at White Sands Missile Range (WSMR), New Mexico, from 2220 to 2300 LST (Local Standard Time). The site is at 1220 m MSL, near the 50-MHz radar located at $32^\circ 24' \text{ N}$, $106^\circ 21' \text{ W}$. Conditions were calm and clear, with a trough in the southwest near the border of Arizona and

California and over northern Mexico. The tropopause height was about 11 km over the site at the time of the measurements. A jet stream existed over northern Mexico.

The data were taken starting from the surface and rising to about 900 m and then returning to the surface. The boundary-layer height had been as large as 2500 m during the day. After sunset, a ground-based inversion formed because of radiational cooling, with cessation in the heating of the mixed layer, such that the turbulence decayed with time while the mean vertical temperature gradient in the residual layer above the nocturnal boundary layer remained nearly adiabatic. Several hours after sunset, the turbulence in the residual layer became very weak, as will be shown in the following.

The USAF and CIRES sensor packages were vertically separated by about 3 m. During the first 600 s (10 min), the combined system was moved up from the ground to about 900 m AGL at 1.5 m s^{-1} . Then the sensors were moved down to about 400 m AGL, where they stayed for a period of 10 min (between 1000 s and 1600 s). After $t = 1600 \text{ s}$, the sensors descended to the ground.

Figure 10 shows three temperature spectra calculated from time series simultaneously measured with three collocated thermometers during the 10-min long period with the blimp at 400 m AGL: the thermocouple (squares), the cold wire (circles), and an inexpensive solid-state thermometer (asterisks). The thermocouple and cold wire spectra show excellent agreement in the frequency range between about 0.1 Hz and 5 Hz. In this range, both spectra follow nicely an inertial-range $f^{-5/3}$ law, and the value of $S_T(f) f^{5/3}$ is $6.2 \times 10^{-5} \text{ K}^2 \text{ Hz}^{2/3}$ in this range. The mean wind velocity during this period was about 5 m s^{-1} , and we obtain $C_T^2 = 2.9 \times 10^{-4} \text{ K}^2 \text{ m}^{-2/3}$. Beyond 5 Hz, the thermocouple spectrum rolls off because of its relatively large thermal mass, while the cold wire spectrum does not show any finite-response effect but starts to flatten close to the Nyquist frequency due to noise. The noise floor of the cold-wire spectrum has been estimated as $S_T^{(n)} = 1 \times 10^{-7} \text{ K}^2 \text{ Hz}^{-1}$.

There are four model spectra in Figure 10: the dashed line is a pure $f^{-5/3}$ law; the three solid lines are models that approximate the three measured spectra, taking into account their respective noise floors and transfer functions; the thermocouple model spectrum is given by (4). In Figure 10, we have used $f_0 = 8 \text{ Hz}$ for the thermocouple model spectrum. The high-pass filtering response function of the cold wire spectrum is modeled with the fourth-order response function $\left[f^4 / f_2^4 (1 + f^4 / f_2^4)^{-1} \right]$, where $f_2 = 0.06 \text{ Hz}$ was chosen. The inexpensive solid-state thermometer has a large thermal inertia ($f_0 = 0.008 \text{ Hz}$) and was sampled only at 0.5 s^{-1} . Its spectrum has a high noise floor ($2 \times 10^{-3} \text{ K}^2 \text{ Hz}^{-1}$), about half of which is due to quantization noise. (The temperature quantization was 0.08 K.)

Figure 11 is the one-sided frequency spectrum of the 10-min-long wind speed time series taken with the hot wire sensor during the same time the temperature data shown in Figure 10 were collected. The noise floor is at about $S_u^{(n)} = 5 \times 10^{-8} \text{ m}^2 \text{ s}^{-2} \text{ Hz}^{-1}$.

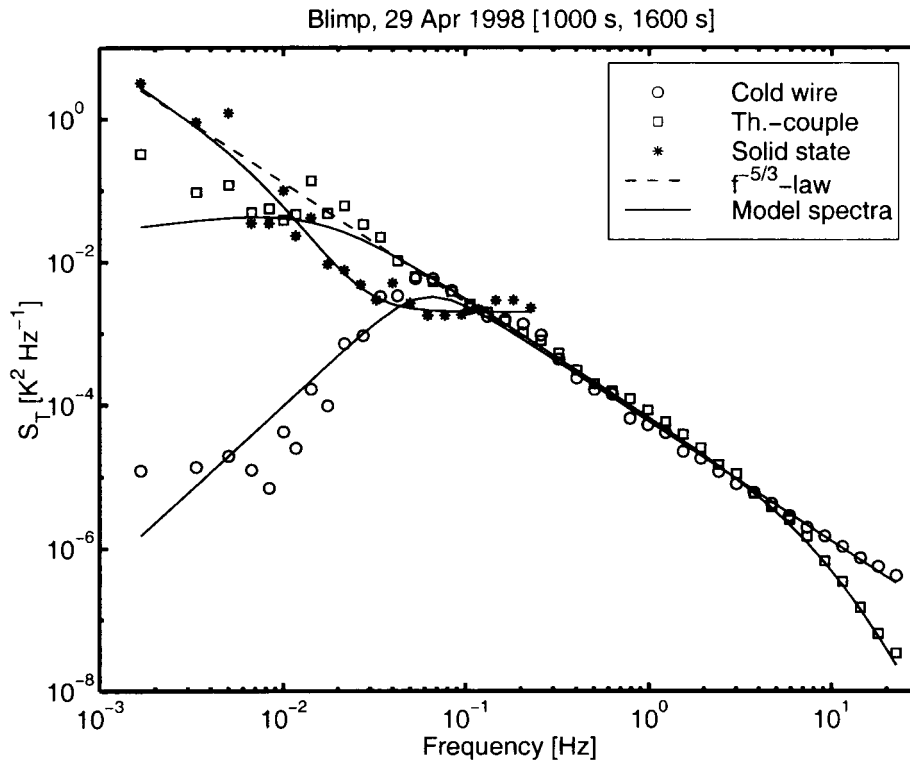


Figure 10. CIRES TLS temperature spectra computed from data simultaneously taken by three collocated thermometers suspended below the CIRES blimp: the USAF cold wire sensor (circles), the CIRES thermocouple sensor (squares), and the solid state thermometer of the basic meteorology payload (asterisks).

4.2. MEASUREMENTS IN AND ABOVE THE CALIFORNIA COAST MARINE LAYER USING HELIPOD

In the following, we present data taken on 8 November 1997 with HELIPOD during the Profiler HELIPOD Intercomparison Experiment (PHELIX), a three-week-long field experiment carried out at Vandenberg Air Force Base (VAFB), California. The main motivation for PHELIX was to collect data that allow the capability of state-of-the-art wind profilers and radio acoustic sounding systems (RASS) to be quantified, particularly in the presence of weak and intermittent turbulence above the California coast marine capping inversion. During PHELIX, HELIPOD was operated simultaneously with three ground-based profiling systems, which were collocated within less than 30 m: the VAFB 449-MHz wind profiler/RASS, the VAFB 915-MHz wind profiler/RASS, and the U.S. Army's 2.9-GHz White Sands Missile Range FMCW radar.

Figure 12 shows the vertical-velocity spectrum, $S_w(f)$, and the temperature spectrum, $S_T(f)$, obtained from a 60-s-long time series of w and T , respectively,

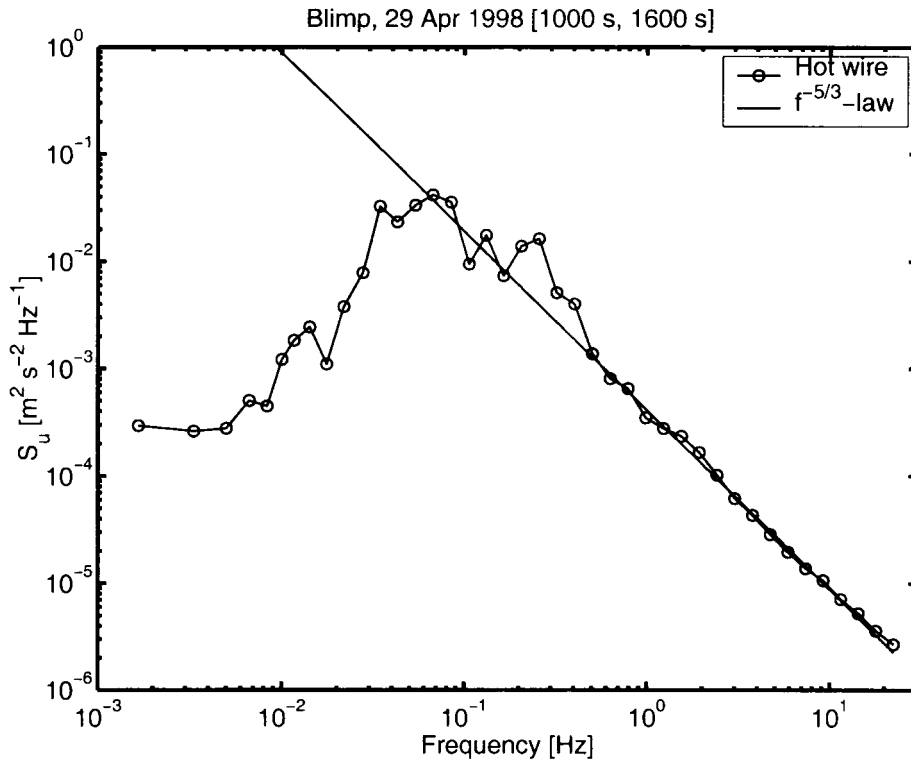


Figure 11. CIRES TLS longitudinal velocity spectrum computed from data taken with the USAF 5- μ m hot-wire sensor during the same time as the data shown in Figure 10.

measured on 8 November 1997 with HELIPOD. The altitude region was between 1380 m MSL and 1470 m MSL, which was in the free troposphere, well above the boundary layer. The elevation of the terrain in the measurement area changes from sea level to a few hundred metres MSL. That is, the data shown in Figure 12 were taken at about 1 km AGL. The noise floors are given in Table I.

Figure 13 shows the vertical temperature (Figure 13a) and zonal velocity profiles (Figure 13b) across an 8-m-thick inversion layer between 1310 m MSL and 1318 m MSL, i.e., in the lower free troposphere. The data were taken along a slanted flight path with a slope of 1/8. The strength of the relatively weak inversion is only 0.7 K. The potential temperature gradient across the layer is $\Delta\Theta/\Delta z = 0.125 \text{ K m}^{-1}$, the zonal wind shear is $\Delta u/\Delta z = 0.12 \text{ s}^{-1}$, and the meridional wind shear (not shown in Figure 13) is $\Delta v/\Delta z = 0.075 \text{ s}^{-1}$. From this, we obtain a gradient Richardson number across the layer of

$$\text{Ri} = \frac{g}{\Theta} \frac{\frac{\Delta\Theta}{\Delta z}}{\left(\frac{\Delta u}{\Delta z}\right)^2 + \left(\frac{\Delta v}{\Delta z}\right)^2} = 0.19, \quad (18)$$

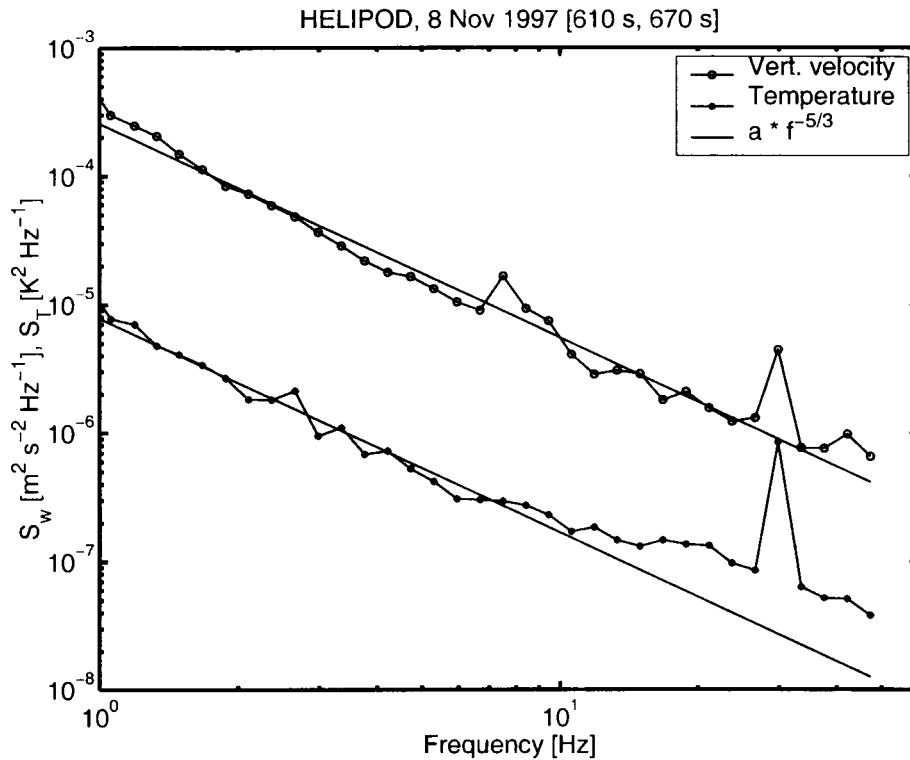


Figure 12. Frequency spectra of a 60-s-long time series of vertical wind velocity, w , and temperature, T , respectively, measured on 8 November 1997 with HELIPOD in the altitude range between 1380 m MSL and 1470 m MSL, well above the California Central Coast marine capping inversion. The noise floors are at about $1 \times 10^{-7} \text{ m}^2 \text{ s}^{-2} \text{ Hz}^{-1}$ and $3 \times 10^{-8} \text{ K}^2 \text{ Hz}^{-1}$, respectively, which at a Nyquist frequency of 50 Hz corresponds to uncorrelated noise standard deviations of 2.2 mm s^{-1} in w and 1.2 mK in T , respectively. The outliers at 30 Hz are due to sound waves from the helicopter rotor.

where g is the acceleration due to gravity.

That is, the gradient Richardson number across the inversion layer is smaller than the critical value of 0.25; thus, one expects the presence of small-scale turbulence within the inversion layer. (Above and below the layer, Ri is much larger than 0.25.) Turbulence is also evident from the relatively large temperature and velocity fluctuations within the layer (Figure 13) and from the observation of turbulent fluxes of heat and zonal momentum against the gradients, i.e., downward, within the inversion layer (Figure 14).

Figure 14 shows preliminary vertical flux profiles of heat (Figure 14a) and zonal momentum (Figure 14b), respectively, calculated from HELIPOD's 100-Hz data of the turbulent fluctuations within the inversion layer. The circles represent values of the local, instantaneous fluxes of heat, $\rho c_p T' w'$, and of zonal momentum, $\rho u' w'$, respectively, where ρ is the air density and $c_p = 1008 \text{ J kg}^{-1} \text{ K}^{-1}$ is the specific heat of dry air at constant pressure. The fluctuations T' , u' , and w' have been cal-

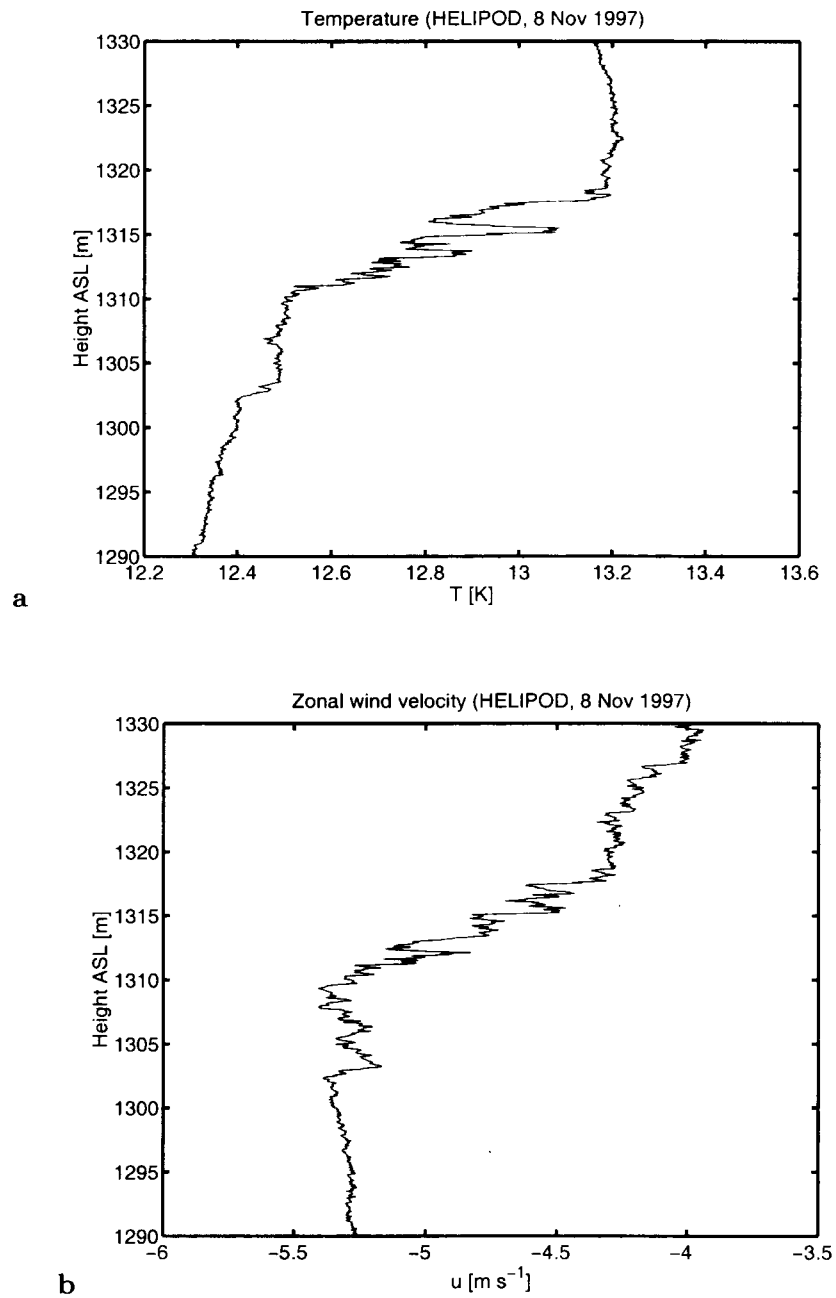


Figure 13. Vertical profiles of temperature (a) and zonal wind velocity (b) within an 8-m-thick inversion layer in the lower free troposphere above the California Coast marine capping inversion. The measurements were taken with HELIPOD during PHELIX on 8 Nov 1997.

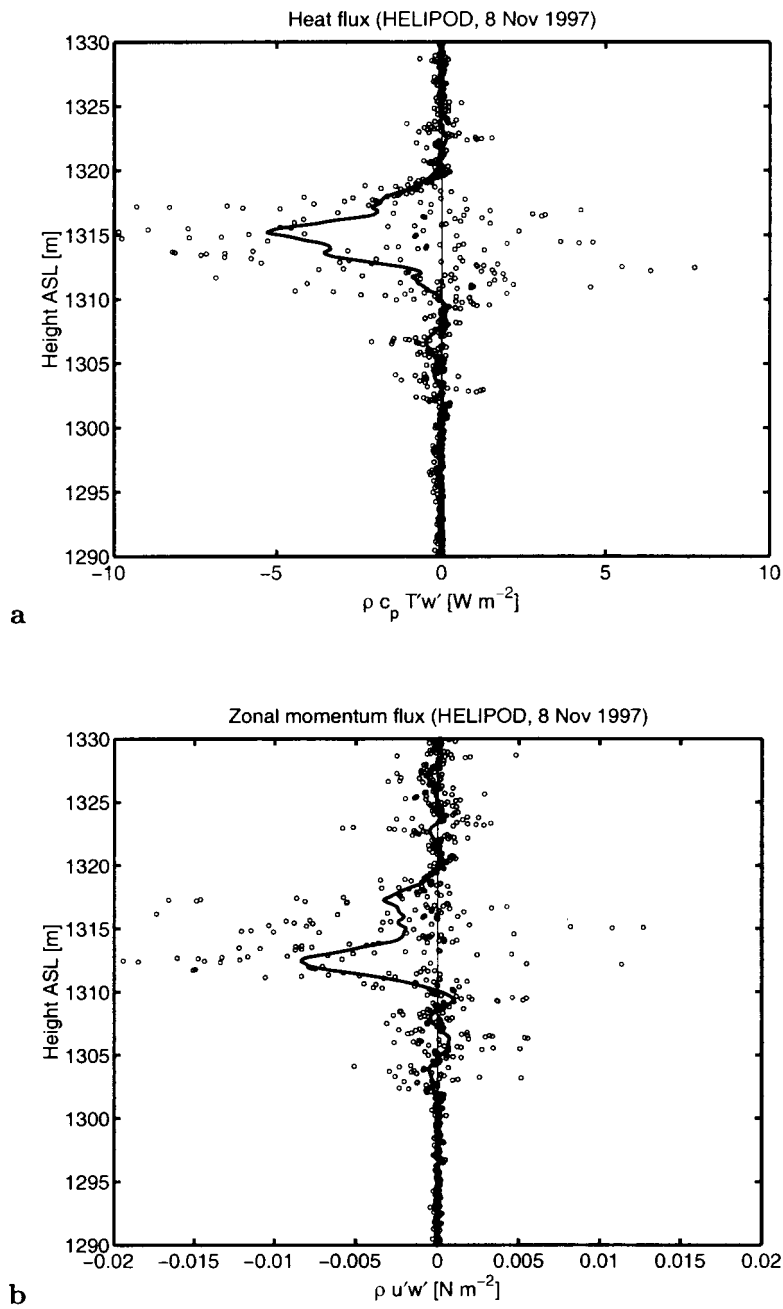


Figure 14. HELIPOD measurements of vertical flux profiles of heat (a) and zonal momentum (b) within the 8-m-thick inversion layer shown in Figure 13.

TABLE I
Noise floors of temperature and wind velocity sensors.

	$S_T^{(n)}$ [K ² Hz ⁻¹]	$S_u^{(n)}$ [m ² s ⁻² Hz ⁻¹]	$S_w^{(n)}$ [m ² s ⁻² Hz ⁻¹]
CIRES TLS	1×10^{-7}	5×10^{-8}	–
HELIPOD	3×10^{-8}	1×10^{-7}	1×10^{-7}

culated by high-pass filtering the measured time series with a triangular window of full width 1 s (100 data points). Since HELIPOD had a forward velocity of about 40 m s⁻¹ and a downward velocity of about 5 m s⁻¹ when penetrating the inversion layer, the temporal window width corresponds to a window width of 40 m horizontally and 5 m vertically. The thick lines represent low-pass filtered (triangular window with full width of 0.5 s in time, 20 m horizontally, and 2.5 m vertically) vertical flux profiles. The heat flux reaches -5 W m^{-2} in the middle of the layer, and the maximum of the magnitude of the downward zonal momentum flux is -0.008 N m^{-2} .

A more complete description of the turbulent fine structure of this inversion will be published elsewhere.

5. Discussion

In the previous section, we presented turbulence measurements taken with the CIRES TLS and HELIPOD in two different field campaigns. The noise floors of the TLS's hot-wire and cold-wire sensors for wind speed and temperature, and of HELIPOD's three-dimensional wind velocity and temperature sensor systems are given in Table I.

Using the detectability criterion stated in Equation (14), we obtain a detectability threshold for the temperature structure parameter as given in the upper part of Table II. We have chosen the two sampling wavelengths $l = 1 \text{ m}$ and $l = 10 \text{ m}$. As typical true air speeds we have assumed $V = 5 \text{ m s}^{-1}$ for the CIRES TLS and $V = 40 \text{ m s}^{-1}$ for HELIPOD.

Correspondingly, the criterion given in Equation (16) leads to estimates for the detectability threshold for the energy dissipation rate as given in the lower part of Table II.

The characteristics shown in Table II qualify the CIRES TLS and HELIPOD as two systems that are very well suited for measuring small-scale turbulence in the stably stratified atmosphere.

TABLE II

Detectability thresholds for temperature structure parameter, $C_{T,\min}^2$, and energy dissipation rate, ϵ_{\min} .

	$l = 1 \text{ m}$	$l = 10 \text{ m}$
$C_{T,\min}^2$ [$\text{K}^2 \text{ m}^{-2/3}$], CIRES TLS ($V = 5 \text{ m s}^{-1}$)	7×10^{-6}	1.5×10^{-7}
$C_{T,\min}^2$ [$\text{K}^2 \text{ m}^{-2/3}$], HELIPOD ($V = 40 \text{ m s}^{-1}$)	1.5×10^{-5}	4×10^{-7}
ϵ_{\min} [$\text{m}^2 \text{ s}^{-3}$], CIRES TLS ($V = 5 \text{ m s}^{-1}$)	2×10^{-9}	7×10^{-12}
ϵ_{\min} [$\text{m}^2 \text{ s}^{-3}$], HELIPOD ($V = 40 \text{ m s}^{-1}$)	1.5×10^{-7}	5×10^{-10}

6. Summary and Conclusions

We have presented technical descriptions of two airborne, state-of-the-art, high-resolution turbulence measurement systems that can be deployed for measuring small-scale turbulence well above the atmospheric surface layer: the CIRES kite and blimp system and the helicopter-borne turbulence measurement system HELIPOD.

In the theoretical part of this paper, we have shown how true air speed, Nyquist frequency, and sensor noise floors limit the detectability of small energy dissipation rates and small temperature structure parameters characterizing small-scale turbulence. We have developed a set of criteria for instrumental requirements that must be fulfilled when measuring weak turbulence as encountered in the stably stratified atmosphere.

In separate case studies, we have analyzed turbulence data from the CIRES TLS and from HELIPOD. We discussed CIRES TLS measurements taken in the residual layer at White Sands Missile Range (29 April 1998), New Mexico, and HELIPOD measurements of turbulence in the free atmosphere above the marine capping inversion at the California Central Coast (8 November 1997, PHELIX, Vandenberg Air Force Base, California).

It has been shown that both the CIRES TLS and HELIPOD are well suited for measuring turbulence that is characterized by very small temperature structure parameters ($10^{-6} \text{ K}^2 \text{ m}^{-2/3}$ and smaller) and very small energy-dissipation rates ($10^{-7} \text{ m}^2 \text{ s}^{-3}$ and smaller). We are not aware of any other turbulence measurement systems that have similar capabilities and can be deployed at altitudes of up to several kilometres.

Appendix A. Relationships between Wavenumber Spectra, Structure Functions, Structure Parameters, and Energy Dissipation Rates

Here we give a concise derivation of the relationships between one-dimensional inertial-range turbulence spectra, one-dimensional structure functions, structure parameters, and energy dissipation rates in the case of very high Reynolds numbers and locally homogeneous and isotropic turbulence.

Consider the one-dimensional autocovariance function $R_q(r)$ of the real variable q , where q is a random function of the spatial coordinate x ,

$$R_q(r) = \langle q(x+r) \cdot q(x) \rangle_x = \int_{-\infty}^{\infty} \Phi_q(k) e^{ikr} dk = \int_0^{\infty} F_q(k) \cos(kr) dk. \quad (19)$$

In the case of statistical stationarity, $R_q(r)$ is even, and the two-sided variance spectrum $\Phi_q(k)$ is real and even. Then the one-sided ($k \geq 0$) variance spectrum can be defined as $F_q(k) = 2\Phi_q(k)$. Integration over all wavenumbers provides the variance of q ,

$$R_q(0) = \sigma_q^2 = \int_0^{\infty} F_q(k) dk. \quad (20)$$

The structure function of q is defined as

$$D_q(r) = \langle [q(x+r) - q(x)]^2 \rangle_x. \quad (21)$$

Assuming an inertial-range spectrum,

$$F_q(k) = c_q k^{-\frac{5}{3}}, \quad (22)$$

writing $D_q(r)$ in the form

$$D_q(r) = 2[R_q(0) - R_q(r)] = 2 \int_0^{\infty} F_q(k) [1 - \cos(kr)] dk, \quad (23)$$

and using the mathematical identity (formula 3.823 on p. 447 in Gradshteyn and Ryzhik (1980))

$$\int_0^{\infty} x^{-\frac{5}{3}} \sin^2(x) dx = \frac{\sqrt{3}\pi}{2^{\frac{4}{3}} \Gamma(\frac{2}{3})} = 1.595, \quad (24)$$

we obtain after some manipulations

$$D_q(r) = \frac{\sqrt{3}\pi}{\Gamma\left(\frac{2}{3}\right)} c_q r^{\frac{2}{3}} = C_q^2 r^{\frac{2}{3}}, \quad (25)$$

where C_q^2 is the turbulence structure parameter of the quantity q . We obtain the one-sided, one-dimensional wavenumber spectrum of the quantity q in terms of the structure parameter,

$$F_q(k) = \frac{\Gamma\left(\frac{2}{3}\right)}{\sqrt{3}\pi} C_q^2 k^{-\frac{5}{3}} = 0.249 C_q^2 k^{-\frac{5}{3}}. \quad (26)$$

In the case of streamwise velocity fluctuations, we have

$$c_u = \alpha_1 \varepsilon^{\frac{2}{3}}, \quad (27)$$

where α_1 is the streamwise Kolmogorov coefficient. This gives

$$C_u^2 = \frac{\sqrt{3}\pi}{\Gamma\left(\frac{2}{3}\right)} \alpha_1 \varepsilon^{\frac{2}{3}}. \quad (28)$$

The spanwise (cross-stream) Kolmogorov coefficient is

$$\alpha_2 = \frac{4}{3} \alpha_1, \quad (29)$$

and we obtain for the structure parameter of the vertical velocity, w ,

$$C_w^2 = \frac{4}{3} \frac{\sqrt{3}\pi}{\Gamma\left(\frac{2}{3}\right)} \alpha_1 \varepsilon^{\frac{2}{3}}. \quad (30)$$

Empirically, it is known that $\alpha_1 \approx 0.5$, which gives

$$C_u^2 \approx 2.0 \varepsilon^{\frac{2}{3}}, \quad \varepsilon \approx 0.35 (C_u^2)^{\frac{3}{2}}, \quad (31)$$

and

$$C_w^2 \approx 2.7 \varepsilon^{\frac{2}{3}}, \quad \varepsilon \approx 0.23 (C_w^2)^{\frac{3}{2}}. \quad (32)$$

Acknowledgements

Data from two field experiments have been presented in this paper: the Profiler HELIPOD Intercomparison Experiment (PHELIX) conducted in November 1997 at the Vandenberg Air Force Base, California, and a field experiment conducted in April 1998 at the White Sands Missile Range, New Mexico. The following organizations and institutions contributed to PHELIX: NOAA's Environmental Technology Laboratory (ETL); NCAR's Atmospheric Technology Division (ATD); NOAA's Forecast Systems Laboratory (FSL); the University of Hannover, Germany; the Deutsche Forschungsgemeinschaft; the U.S. Air Force; the U.S. Army; and Aerodata Flugmeßtechnik GmbH, Braunschweig, Germany. We thank Don Lenschow and an anonymous reviewer for their valuable comments. Thanks are also due to Holger Siebert who brought an error in two equations in an earlier version of the manuscript to the authors' notice.

References

- Angevine, W. M., Bakwin, P. S., and Davis, K. J.: 1998, 'Wind Profiler and RASS Measurements Compared with Measurements from a 450-m-tall Tower', *J. Atmos. Oceanic Tech.* **15**, 818–825.
- Balsley, B. B., Jensen, M. L., and Frehlich, R. G.: 1998, 'The Use of State-of-the-Art Kites for Profiling the Lower Atmosphere', *Boundary-Layer Meteorol.* **87**, 1–25.
- Balsley, B. B., Williams, J. B., Tyrrell, G. W., and Balsley, C. L.: 1992, 'Atmospheric Research Using Kites: Here We Go Again!', *Bull. Amer. Meteorol. Soc.* **73**, 17–29.
- Batchelor, G. K.: 1953, *The Theory of Homogeneous Turbulence*, Cambridge University Press, Cambridge, 197 pp.
- Bruun, H. H.: 1995, *Hot-Wire Anemometry, Principles and Signal Analysis*, Oxford University Press, Oxford, 536 pp.
- Buck, A. L.: 1976, 'The Variable-Path Lyman-Alpha Hygrometer and its Operating Characteristics', *Bull. Amer. Meteorol. Soc.* **57**, 1113–1118.
- Cardell, G.: 1993, 'A Note on the Temperature-Dependent Hot-Wire Calibration Method of Cimbala and Park', *Exp. Fluids* **14**, 283–285.
- Cimbala, J. M. and Park, W. J.: 1990, 'A Direct Hot-Wire Calibration Technique to Account for Ambient Temperature Drift in Incompressible Flow', *Exp. Fluids* **8**, 299–300.
- Crawford, T. L. and Dobosy, R. J.: 1972, 'A Sensitive Fast-Response Probe to Measure Turbulence and Heat Flux from any Airplane', *Boundary-Layer Meteorol.* **59**, 257–278.
- Eaton, F. D., Nastrom, G. D., Masson, B., Hahn, I., McCrae, K., Novlin, S. R., and Berkopec, T.: 1998, 'Radar and Aircraft Observations of a Layer of Strong Refractivity Turbulence', *Proc. SPIE Vol. 3381*, Orlando, FL, pp. 230–238.
- Friehe, C. A.: 1986, 'Fine-Scale Measurements of Velocity, Temperature, and Humidity in the Atmospheric Boundary Layer', in D. H. Lenschow (ed.), *Probing the Atmospheric Boundary Layer*, Amer. Meteorol. Soc., Boston, pp. 29–38.
- Gradshteyn, I. S. and Ryzhik, I. M.: 1980, *Table of Integrals, Series, and Products*, Academic Press, New York, 1160 pp.
- Hahn, I. L., Venet, B. P., Eaton, F. D., Hugo, R. J., and Novlin, S. R.: 1999, 'Refractive Index Structure Parameter in the Boundary Layer as Measured from an Aircraft and a Ground Based Scintillometer', in *Preprints of the 13th Symposium on Boundary Layers and Turbulence*, Dallas, TX, 10–15 January 1999, pp. 139–142.

- Hauf, T.: 1984, 'Turbulenzmessungen mit dem Forschungsflugzeug Falcon', *Met. Rdsch.* **37**, 163–176.
- Hugo, R., Nowlin, S. R., Eaton, F. D., Bishop, K. P., and McCrae, K. A.: 1999, 'Hot-Wire Calibration in a Non-Isothermal Incompressible Pressure Variant Flow', *International Symposium on AeroSense*, Orlando, FL, 5–9 April 1999, *Proc. SPIE*, Vol. 3706, pp. 11–22.
- Kaimal, J. C.: 1986, 'Flux Profile Measurements from Towers in the Boundary Layer', in D. H. Lenschow (ed.), *Probing the Atmospheric Boundary Layer*, Amer. Meteorol. Soc., Boston, pp. 19–28.
- Kaimal, J. C. and Gaynor, J. E.: 1983, 'The Boulder Atmospheric Observatory', *J. Clim. Appl. Meteorol.* **22**, 863–880.
- Kaimal, J. C., Wyngaard, J. C., Haugen, D. A., Coté, O. R., and Izumi, Y.: 1976, 'Turbulence Structure in the Convective Boundary Layer', *J. Atmos. Sci.* **33**, 2152–2169.
- Kaimal, J. C., Wyngaard, J. C., Izumi, Y., and Coté, O. R.: 1972, 'Spectral Characteristics of Surface-Layer Turbulence', *Quart. J. Roy. Meteorol. Soc.* **98**, 563–589.
- King, L. V.: 1914, 'On the Convection of Heat from Small Cylinders in a Stream of Fluid: Determination of the Convection Constants of Small Platinum Wires with Applications to Hot-Wire Anemometry', *Phil. Trans. Roy. Soc. London, Ser. A* **214**, 373–432.
- Knapp, K. G., Jensen, M. L., Balsley, B. B., Bognar, J. A., Oltmans, S. J., Smith, T. W., and Birks, J. W.: 1998, 'Vertical Profiling Using Complementary Kite and Tethered Balloon Platforms at Ferryland Downs, Newfoundland, Canada: Observation of a Dry, Ozone-Rich Plume in the Free Troposphere', *J. Geophys. Res.* **103**, 13,389–13,397.
- Lenschow, D. H.: 1972, 'The Measurement of Air Velocity and Temperature Using the NCAR Buffalo Aircraft System', *NCAR-TN/EDD-74*, National Center for Atmospheric Research, Boulder, CO, 39 pp.
- Lenschow, D. H.: 1986, 'Aircraft Measurements in the Boundary Layer', in D. H. Lenschow (ed.), *Probing the Atmospheric Boundary Layer*, Amer. Meteorol. Soc., Boston, pp. 39–55.
- Masson, B., Scruggs, B., Hayes, M., Wissler, J., Bishop, K., and Kyrakis, D.: 1996, 'Airborne Measurements of Tropopause Temperature Fluctuations', in *AIAA 34th Aerospace Sciences Meeting and Exhibit*, Reno, Nevada, Jan. 15–18 1996, AIAA Paper 96-0265.
- Monin, A. S. and Yaglom, A. M.: 1975, *Statistical Fluid Mechanics*, Vol. 2, MIT Press, Cambridge, MA, 769 pp.
- Muschinski, A. and Wode, C.: 1998, 'First In-Situ Evidence for Coexisting Submeter Temperature and Humidity Sheets in the Lower Free Troposphere', *J. Atmos. Sci.* **55**, 2893–2906.
- Nagano, Y. and Tsuji, T.: 1994, 'Recent Developments in Hot- and Cold-Wire Techniques for Measurements in Turbulent Shear Flows near Walls', *Exp. Thermal Fluid Sci.* **9**, 94–110.
- Ogawa, Y. and Ohara, T.: 1982, 'Observation of the Turbulent Structure in the Planetary Boundary Layer with a Kytoon-Mounted Ultrasonic Anemometer System', *Boundary-Layer Meteorol.* **22**, 123–131.
- Oppenheim, A. V. and Schaffer, R. W.: 1975, *Digital Signal Processing*, Prentice-Hall, Inc., Englewood Cliffs, NJ, 585 pp.
- Paranthoen, P., LeCordier, J. C., and Petit, C.: 1983, 'Dynamic Sensitivity of the Constant-Temperature Hot-Wire Anemometer to Temperature Fluctuations', *TSI Quarterly* **9**(3), 3–8.
- Paranthoen, P., Petit, C., and LeCordier, J. C.: 1982, 'The Effect of the Thermal Prong-Wire Interaction on the Response of a Cold Wire in Gaseous Flows (Air, Argon and Helium)', *J. Fluid Mech.* **124**, 457–473.
- Redeker, A. and Vörsmann, P.: 1985, 'Precise Vertical Speed Reconstruction Based on Vertical Acceleration and Barometric Altitude', *Z. Flugwiss. Weltraumforsch.* **9**, 243–251.
- Taylor, G. I.: 1938, 'The Spectrum of Turbulence', *Proc. Roy. Soc. London, Ser. A* **164**, 476–490.
- Tsuji, T., Nagano, Y., and Tagawa, M.: 1992, 'Frequency Response and Instantaneous Temperature Profile of Cold-Wire Sensors for Fluid Temperature Fluctuation Measurements', *Exp. Fluids* **13**, 171–178.

- Vörsmann, P.: 1984, *Ein Beitrag zur bordautonomen Windmessung*, Ph.D. Dissertation, Technical University of Braunschweig, Braunschweig, 135 pp.
- Wyngaard, J. C.: 1986, 'Measurement Physics', in D. H. Lenschow (ed.), *Probing the Atmospheric Boundary Layer*, Amer. Meteorol. Soc., Boston, pp. 5–18.